

Dispersive Analysis of Low Energy $\gamma N \rightarrow \pi N$ Process and Studies on the $N^*(890)$ Resonance

YAO MA¹, WEN-QI NIU¹, DE-LIANG YAO², AND HAN-QING ZHENG^{1,3}

¹*Department of Physics and State Key Laboratory of Nuclear Physics and Technology, Peking University, Beijing 100871, P. R. China*

²*School of Physics and Electronics, Hunan University, Changsha 410082, P. R. China*

³*Collaborative Innovation Center of Quantum Matter, Beijing, Peoples Republic of China*

August 18, 2020

Abstract

We present a dispersive representation of the $\gamma N \rightarrow \pi N$ partial-wave amplitude based on unitarity and analyticity. In this representation, the right-hand-cut contribution responsible for πN final-state-interaction effects are taken into account via an Omnés formalism with elastic πN phase shifts as inputs, while the left-hand-cut contribution is estimated by invoking chiral perturbation theory. Numerical fits are performed in order to pin down the involved subtraction constants. It is found that good fit quality can be achieved with only one free parameter and the experimental data of the multipole amplitude E_0^+ in the energy region below the $\Delta(1232)$ are well described. Furthermore, we extend the $\gamma N \rightarrow \pi N$ partial-wave amplitude to the second Riemann sheet so as to extract the couplings of the $N^*(890)$. The modulus of the residue of the multipole amplitude E_0^+ ($S_{11}pE$) is $2.41 \text{ mfm} \cdot \text{GeV}^2$ and the partial width of $N^*(890) \rightarrow \gamma N$ at the pole is about 0.369 MeV , which is almost the same as the one of the $N^*(1535)$ resonance, indicating that $N^*(890)$ strongly couples to πN system.

1 Introduction

Single pion photoproduction off the nucleon has been extensively studied for its importance in determining the spectrum and properties of the nucleon resonances [1–4]. There have been many measurements on this process, accumulating a wealth of experimental data on, e.g., cross section, photon asymmetry, target asymmetry, etc; see e.g. Refs [5–9]. Based on the dataset, partial wave analyses were performed to anatomize the underlying structure of the reaction amplitude and justify the existence of the nucleon resonances theoretically. At low energies, it has been successful to explore the photoproduction processes in chiral perturbation theory (ChPT) [10–17]. In combination of unitarization approaches [18], the valid region of the chiral amplitudes is extended and physical states behave themselves as pole singularities of the unitarized amplitudes. Nevertheless, most of the unitarization methods only take the unitary cut into account, while the remaining left-hand cuts (l.h.c.s) are left out, leading to the drawback that the proper analytic and crossing properties of the amplitude is not faithfully guaranteed. In consequence, spurious poles arise to mimic the contribution of the left-hand cuts, or even worse, prevent us from discovering certain truly existent poles, e.g. virtual poles or subthreshold resonances.

In Refs. [19–21], a novel subthreshold resonance named $N^*(890)$ was found in the S_{11} wave through a prudent analysis of the covariant chiral amplitude of πN scattering [22–25] by applying the method of Peking University (PKU) representation [26–31]. The PKU representation respects causality and has already been used to establish the existences of the σ and κ states [26, 28]. The discovery of the $N^*(890)$ resonance is nothing but an improved implement of analyticity compared to other unitarization methods. For instance, it is pointed out in Ref. [32] that the $N^*(890)$ resonance still exists even in a K -matrix parametrization if a better treatment of analyticity is executed. However, it should be emphasized that, in the traditional K matrix method without any improvement of analyticity, even if a pole emerges from the background polynomial, it is not legitimate to discuss whether it is physical or not, it only means the non-background part of the K matrix parametrization is incomplete in characterizing whole physics. In PKU representation, the existence of $N^*(890)$ actually only depends on our understanding or knowledge of left hand cut contribution at qualitative level – that is its contribution to the phase shift is negative. In this paper, we intend to explore the $N^*(890)$ resonance in the $\gamma N \rightarrow \pi N$ scattering to gain more information on its properties.

Our $\gamma N \rightarrow \pi N$ amplitudes are obtained through a dispersive representation, which is set up with the help of unitarity and analyticity [33–36]. The inputs of the dispersive representation are πN final-state-interaction amplitude and chiral tree-level $\gamma N \rightarrow \pi N$ amplitude estimating the left hand singularities of pion photoproduction. In a single channel approximation, the former can be achieved by an Omnès solution with the πN scattering phase as input. The left hand cuts are calculated based on a chiral Lagrangian with pion and nucleon fields truncated at order q^2 . We review the analytic structures of pion photoproduction amplitudes in Ref. [37] and analyze the relevant singularities to arising in our calculation. In addition, we find that kinematical singularities in this inelastic process are rather complicated. Cuts coming from kinematical structure depend on how to organize the analytic functions in the amplitudes. These cuts could be in the complex plane and may affect the residues of $N^*(890)$. To avoid such complexity, we deform these cuts in a particular way to make sure that they are lying on the real axis, below the pseudo threshold of πN scattering.

We fit the multipole amplitudes E_{0+} (S_{11pE} and S_{11nE}) from Ref. [38] below the $\Delta(1232)$ peak in order to determine the subtraction polynomial in the dispersive representation. The residue couplings of $N^*(890)$ can be computed by analytic continuation of the amplitude to second sheet, in which the PKU representation of πN \mathcal{S} matrix is employed. We compare the residues of $N^*(890)$ extracted from multipole amplitudes with the ones of $N^*(1535)$ obtained in Ref. [39] to learn the properties of $N^*(890)$ and get some information of structures by analogy with the analysis of $N^*(1535)$.

The structure of this paper is organized as follows. In Section 2 we set up the dispersive formalism for $\gamma N \rightarrow \pi N$ process. Then the left-hand-cuts are estimated based on chiral perturbation theory in Section 3, and we also make an analysis about the singularities which will appear in this pion photoproduction process. In last two sections, numerical results are carried out and summary is presented.

2 Dispersive formalism for $\gamma N \rightarrow \pi N$

2.1 Dispersive representation

The unitarity relation for the $\gamma N \rightarrow \pi N'$ partial wave amplitude reads

$$\frac{\mathcal{M}(s+i\epsilon) - \mathcal{M}(s-i\epsilon)}{2i} = \text{Im}\mathcal{M}(s+i\epsilon) = \mathcal{T}^*(s+i\epsilon)\rho(s+i\epsilon)\mathcal{M}(s+i\epsilon), \quad (1)$$

where \mathcal{T} is pion-nucleon scattering amplitude in S_{11} wave. The function $\rho(s)$ is defined by

$$\rho(s) = \frac{\sqrt{(s-s_L)(s-s_R)}}{s}, \quad (2)$$

where $s_R \equiv (m_N + m_\pi)^2$ and $s_L \equiv (m_N - m_\pi)^2$. Equivalently, Eq. (1) can be recast to

$$\mathcal{M}(s+i\epsilon) = \mathcal{S}(s+i\epsilon)\mathcal{M}(s-i\epsilon), \quad (3)$$

where $\mathcal{S}(s) = 1 + 2i\rho(s)\mathcal{T}(s)$ which is the πN scattering S matrix in single channel case. The scattering amplitude \mathcal{M} may be separated into two parts, i.e., $\mathcal{M} = \mathcal{M}_R + \mathcal{M}_L$. The former part \mathcal{M}_R only contains the right hand cut (RHC) starting at s_R , while the latter part \mathcal{M}_L is free of RHC singularity. Substituting $\mathcal{M} = \mathcal{M}_R + \mathcal{M}_L$ into Eq. (3), one gets

$$\mathcal{M}_R^+ = \mathcal{S}\mathcal{M}_R^- + (\mathcal{S} - 1)\mathcal{M}_L. \quad (4)$$

For convenience, the abbreviations $\mathcal{M}^\pm(s) = \lim_{\epsilon \rightarrow 0} \mathcal{M}(s \pm i\epsilon)$ have been used. To proceed, we introduce a helper function $\mathcal{D}(s)$ which is analytic throughout the complex s plane but encodes the same unitarity singularity as $\mathcal{M}(s)$. Namely, it satisfies the same unitarity condition as $\mathcal{M}(s)$ along the unitary cut:

$$\frac{\mathcal{D}^+}{\mathcal{D}^-} = \frac{\mathcal{M}^+}{\mathcal{M}^-} = \mathcal{S}. \quad (5)$$

By expressing the \mathcal{S} matrix in Eq. (4) by $\mathcal{D}(s)$, the following relation of spectral functions can be obtained:

$$\text{Im}(\mathcal{D}^{-1}\mathcal{M}_R) = -(\text{Im}\mathcal{D}^{-1})\mathcal{M}_L. \quad (6)$$

Straightforwardly, a dispersive representation for \mathcal{M}_R can be written down,

$$\mathcal{M}_R(s) = \mathcal{D} \left(-\frac{s^n}{\pi} \int_{s_R}^{\infty} \frac{(\text{Im}\mathcal{D}^{-1})\mathcal{M}_L}{s'^n(s'-s)} ds' + \mathcal{P} \right), \quad (7)$$

where n is the number of subtractions and $\mathcal{P}(s)$ is subtraction polynomial. Eventually,

$$\mathcal{M}(s) = \mathcal{M}_L + \mathcal{D} \left(-\frac{s^n}{\pi} \int_{s_R}^{\infty} \frac{(\text{Im}\mathcal{D}^{-1})\mathcal{M}_L}{s'^n(s'-s)} ds' + \mathcal{P} \right). \quad (8)$$

Thus, the pion photoproduction amplitude $\mathcal{M}(s)$ is determined up to a polynomial, once $\mathcal{D}(s)$ and $\mathcal{M}_L(s)$ are known.

Based on the unitarity condition in Eq. (5), one can write a spectral representation for the auxiliary function $\mathcal{D}(s)$,

$$\mathcal{D}(s) = \frac{1}{\pi} \int_{s_R}^{\infty} \frac{\mathcal{T}^*(s)\rho(s')\mathcal{D}(s')}{s'-s} ds'. \quad (9)$$

The above representation yields an integral equation for $\mathcal{D}(s)$, which has the so-called Omnés solution [40]

$$\mathcal{D}(s) = \tilde{\mathcal{P}}(s) \exp \left[\frac{s}{\pi} \int_{s_R}^{\infty} \frac{\delta(s')}{s'(s'-s)} ds' \right] \quad (10)$$

with $\tilde{\mathcal{P}}$ standing for zero points in complex plane and $\delta(s)$ being the elastic πN phase shift, in accordance with the Watson final state interaction (FSI) theorem [41].

3 Estimate on the left-hand-cut contribution in ChPT

3.1 Basics of single one-pion photoproduction off the nucleon

Single one-pion photoproduction off the nucleon ($\gamma N \rightarrow \pi N$) is the process as described by

$$\gamma(q) + N(p) \rightarrow \pi^a(q') + N'(p') , \quad (11)$$

where a is the isospin index of the pion and momenta of the particles are indicated in the parentheses. The isospin structure of the scattering amplitude can be written as

$$\mathcal{M}(\gamma + N \rightarrow \pi^a + N') = \chi'_N \left\{ \delta_{a3} \mathcal{M}^+ + \frac{1}{2} [\tau_a, \tau_3] \mathcal{M}^- + \tau_3 \mathcal{M}^0 \right\} \chi_N , \quad (12)$$

where τ_a ($a = 1, 2, 3$) are Pauli matrices in isospin space. Amplitudes with definite isospin $I = \frac{1}{2}, \frac{3}{2}$ can be obtained from \mathcal{M}^\pm and \mathcal{M}^0 via ^{1 2}

$$\mathcal{M}^{I=\frac{3}{2}} = \sqrt{\frac{2}{3}} (\mathcal{M}^+ - \mathcal{M}^-) , \quad (13)$$

$$\mathcal{M}^{I=\frac{1}{2}} = -\frac{1}{\sqrt{3}} (\mathcal{M}^+ + 2\mathcal{M}^- + 3\mathcal{M}^0) , \quad (p \text{ target}) \quad (14)$$

$$\mathcal{M}^{I=\frac{1}{2}} = \frac{1}{\sqrt{3}} (\mathcal{M}^+ + 2\mathcal{M}^- - 3\mathcal{M}^0) , \quad (n \text{ target}) . \quad (15)$$

The isospin amplitudes \mathcal{M}^I with either $I = \frac{1}{2}, \frac{3}{2}$ or $I = \pm, 0$ can be further decomposed in terms of four independent Lorentz operators as

$$\mathcal{M}^I(s, t) \equiv \bar{u}(p') \mathcal{T}^I u(p) = \bar{u}(p') \left[\sum_{i=1}^4 \mathcal{A}_i^I(s, t) L_\mu^i \epsilon^\mu \right] u(p) , \quad (16)$$

where

$$\begin{aligned} L_\mu^1 &= i\gamma_5 \gamma_\mu \gamma \cdot q , \\ L_\mu^2 &= 2i\gamma_5 (P_\mu q \cdot q' - q'_\mu P \cdot q) , \\ L_\mu^3 &= \gamma_5 (\gamma_\mu q' \cdot q - q'_\mu \gamma \cdot q) , \\ L_\mu^4 &= 2\gamma_5 (\gamma_\mu P \cdot q - P_\mu \gamma \cdot q) . \end{aligned} \quad (17)$$

Note that the operators L_μ^i obey the Ward identity [1]. Here ϵ_μ is the polarization vector of the photon, $u(p)$ and $\bar{u}(p')$ are the spinors of the nucleons.

3.2 Calculation of chiral amplitudes at tree level

The effective Lagrangian for our calculation of the chiral amplitude up to $\mathcal{O}(p^2)$ reads

$$\mathcal{L}_{\text{eff}} = \mathcal{L}_{\pi N}^{(1)} + \mathcal{L}_{\pi N}^{(2)} + \mathcal{L}_{\pi\pi}^{(2)} \quad (18)$$

¹The convention in Ref. [42] is adopted for the CG coefficients and for the physical pion states we use $\pi^+ = -\frac{1}{\sqrt{2}}(\pi_1 - i\pi_2)$ and $\pi^- = \frac{1}{\sqrt{2}}(\pi_1 + i\pi_2)$.

² \mathcal{M} and \mathcal{P} are actually vectors with two components in isospin space of $I = \frac{1}{2}$ channel due to target asymmetry caused by electromagnetic interaction.

with the superscripts referring to chiral orders. The terms in the above equation are given by [43]

$$\mathcal{L}_{\pi N}^{(1)} = \bar{\Psi} \left(i\not{D} - m + \frac{g}{2} \gamma^\mu \gamma_5 u_\mu \right) \Psi , \quad (19)$$

$$\mathcal{L}_{\pi N}^{(2)} = \bar{\Psi} \sigma^{\mu\nu} \left[\frac{c_6}{2} f_{\mu\nu}^+ + \frac{c_7}{2} v_{s,\mu\nu} \right] \Psi ,$$

$$\mathcal{L}_{\pi\pi}^{(2)} = \frac{F^2}{4} \text{Tr} \left[D_\mu U (D^\mu U)^\dagger \right] + \frac{F^2}{4} \text{Tr} (\chi U^\dagger + U \chi^\dagger) , \quad (20)$$

where m , g and F are nucleon mass, nucleon axial coupling and pion decay constant in the chiral limit, in order. Given our working accuracy, they are set equal to their physical counterparts, m_N , g_A and F_π , the physical nucleon mass, physical axial charge and pion decay constants. Namely, $m = m_N$, $g = g_A$ and $F = F_\pi$. Here c_6 and c_7 are $\mathcal{O}(p^2)$ low energy constants (LECs) which are known parameters to be determined by experimental data; See Ref. [43] for definitions of the chiral blocks.

The relevant pieces extracted from the expanded form of the Lagrangians in Eq. (19) are

$$\mathcal{L}_{\pi N}^{(1)} \supset + \frac{g_A}{2F_\pi} \partial_\mu \phi \bar{\Psi} \gamma_5 \gamma^\mu \Psi - \frac{e}{2} A_\mu \bar{\Psi} [\gamma^\mu (\tau_3 + 1)] \Psi - i \frac{eg_A}{4F_\pi} A_\mu \bar{\Psi} (\gamma_5 \gamma^\mu [\phi, \tau_3]) \Psi , \quad (21)$$

$$\mathcal{L}_{\pi N}^{(2)} \supset - e \bar{\Psi} \sigma^{\mu\nu} \left[\frac{c_6}{2} (\partial_\mu A_\nu - \partial_\nu A_\mu) \tau_3 + \frac{c_7}{4} (\partial_\mu A_\nu - \partial_\nu A_\mu) \right] \Psi , \quad (22)$$

$$\mathcal{L}_{\pi\pi}^{(2)} \supset - \frac{i\epsilon}{8} A^\mu \text{Tr} (\{\partial_\mu \phi, [\phi, \tau_3]\}) . \quad (23)$$

Tree-level Feynman diagrams up to $\mathcal{O}(q^2)$ are displayed in Figures 1 and 2.

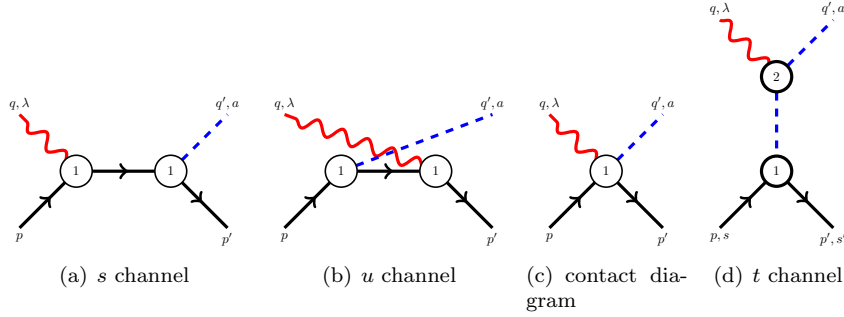


Figure 1: $\mathcal{O}(p)$ diagram

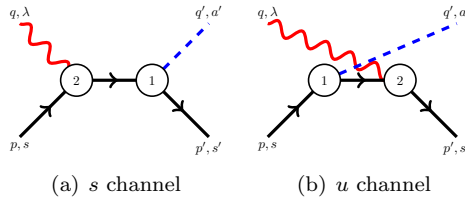


Figure 2: $\mathcal{O}(p^2)$ diagram

The full amplitude reads

$$i\mathcal{M}^{(1)} = \frac{eg_A}{4F_\pi} \chi_f^\dagger [\tau_a, \tau_3] \chi_i \bar{u}_{s'}(p') \gamma_5 \gamma^\mu u_s(p) \epsilon_{\lambda,\mu}(q)$$

$$\begin{aligned}
& + \frac{ieg_A}{4F_\pi} \chi_f^\dagger \tau_a (\tau_3 + 1) \chi_i \bar{u}_{s'}(p') \gamma_5 \gamma^\nu \frac{i}{\not{p} + \not{q} - m_N + i\epsilon} \gamma^\mu u_s(p) q'_\nu \epsilon_{\lambda,\mu}(q) \\
& + \frac{ieg_A}{4F_\pi} \chi_f^\dagger (\tau_3 + 1) \tau_a \chi_i \bar{u}_{s'}(p') \gamma^\mu \frac{i}{\not{p}' - \not{q} - m_N + i\epsilon} \gamma_5 \gamma^\nu u_s(p) q'_\nu \epsilon_{\lambda,\mu}(q) \\
& - \frac{ieg_A}{4F_\pi} \chi_f^\dagger [\tau_a, \tau_3] \chi_i \epsilon_\lambda^\nu(q) q'_\nu \bar{u}_{s'}(p') \gamma_5 \gamma^\mu u_s(p) \frac{i(p'_\mu - p_\mu)}{(p' - p)^2 - m_\pi^2 + i\epsilon} \\
& + \frac{ieg_A}{4F_\pi} \chi_f^\dagger [\tau_a, \tau_3] \chi_i \epsilon_\lambda^\nu(q) \bar{u}_{s'}(p') \gamma_5 \gamma^\mu u_s(p) \frac{i(p'_\nu - p_\nu)(p'_\mu - p_\mu)}{(p' - p)^2 - m_\pi^2 + i\epsilon}, \tag{24}
\end{aligned}$$

$$\begin{aligned}
i\mathcal{M}^{(2)} & = \frac{-eg_A}{2F_\pi} \chi_f^\dagger \tau_a \left[\frac{c_6}{2} (q_\nu \epsilon_{\mu,\lambda}(q) - q_\mu \epsilon_{\nu,\lambda}(q)) \tau_3 \right. \\
& \quad \left. + \frac{c_7}{4} (q_\nu \epsilon_{\mu,\lambda}(q) - q_\mu \epsilon_{\nu,\lambda}(q)) \right] \chi_i q'^\rho \bar{u}_{s'}(p') \gamma_5 \gamma_\rho \frac{i}{(\not{q} + \not{p}) - m_N + i\epsilon} \sigma^{\mu\nu} u_s(p) \\
& + \frac{-eg_A}{2F_\pi} \chi_f^\dagger \left[\frac{c_6}{2} (q_\nu \epsilon_{\mu,\lambda}(q) - q_\mu \epsilon_{\nu,\lambda}(q)) \tau_3 \right. \\
& \quad \left. + \frac{c_7}{4} (q_\nu \epsilon_{\mu,\lambda}(q) - q_\mu \epsilon_{\nu,\lambda}(q)) \right] \tau_a \chi_i q'^\rho \bar{u}_{s'}(p') \sigma^{\mu\nu} \frac{i}{(\not{p} - \not{q}') - m_N + i\epsilon} \gamma_5 \gamma_\rho u_s(p), \tag{25}
\end{aligned}$$

where superscript stands for chiral order. Now those invariant scalar functions can be extracted from the above amplitudes:

$$\begin{aligned}
\mathcal{A}_1^+ & = -\frac{ieg_A m_N}{2F_\pi} \left(\frac{1}{u - m_N^2} + \frac{1}{s - m_N^2} \right) - \frac{ieg_A c_6}{F} \left(\frac{2m_N^2}{u - m_N^2} + \frac{2m_N^2}{s - m_N^2} + 1 \right), \\
\mathcal{A}_1^0 & = -\frac{ieg_A m_N}{2F_\pi} \left(\frac{1}{u - m_N^2} + \frac{1}{s - m_N^2} \right) - \frac{ieg_A c_7}{2F} \left(\frac{2m_N^2}{u - m_N^2} + \frac{2m_N^2}{s - m_N^2} + 1 \right), \\
\mathcal{A}_1^- & = -\frac{ieg_A m_N}{2F_\pi} \left(-\frac{1}{u - m_N^2} + \frac{1}{s - m_N^2} \right) - \frac{ieg_A c_6}{F} \left(-\frac{2m_N^2}{u - m_N^2} + \frac{2m_N^2}{s - m_N^2} \right), \\
\mathcal{A}_2^+ & = \frac{ieg_A m_N}{4F_\pi P \cdot q} \left(\frac{1}{u - m_N^2} - \frac{1}{s - m_N^2} \right), \\
\mathcal{A}_2^0 & = \frac{ieg_A m_N}{4F_\pi P \cdot q} \left(\frac{1}{u - m_N^2} - \frac{1}{s - m_N^2} \right), \\
\mathcal{A}_2^- & = -\frac{ieg_A m_N}{4F_\pi P \cdot q} \left(\frac{1}{u - m_N^2} + \frac{1}{s - m_N^2} + \frac{4}{t - m_\pi^2} \right), \\
\mathcal{A}_3^+ & = \frac{eg_A c_6 m_N}{F_\pi} \left(\frac{1}{u - m_N^2} - \frac{1}{s - m_N^2} \right), \\
\mathcal{A}_3^0 & = \frac{eg_A c_7 m_N}{2F_\pi} \left(\frac{1}{u - m_N^2} - \frac{1}{s - m_N^2} \right), \\
\mathcal{A}_3^- & = \frac{eg_A c_6 m_N}{F_\pi} \left(-\frac{1}{u - m_N^2} - \frac{1}{s - m_N^2} \right), \\
\mathcal{A}_4^+ & = -\frac{eg_A c_6 m_N}{F_\pi} \left(\frac{1}{u - m_N^2} + \frac{1}{s - m_N^2} \right), \\
\mathcal{A}_4^0 & = -\frac{eg_A c_7 m_N}{2F_\pi} \left(\frac{1}{u - m_N^2} + \frac{1}{s - m_N^2} \right), \tag{26}
\end{aligned}$$

$$\mathcal{A}_4^- = -\frac{e g_A c_6 m_N}{F_\pi} \left(-\frac{1}{u - m_N^2} + \frac{1}{s - m_N^2} \right). \quad (27)$$

3.3 Partial wave projection

It is convenient to perform partial wave projection using the helicity formalism proposed in Ref. [44]. To that end, one can substitute the photon polarization vector $\epsilon_\mu(q)$, the nucleon spinors $u(p)$ and $\bar{u}(p')$ in Eq. (16) by their helicity eigenstates $\epsilon_\mu(q, \lambda_2)$, $u(p, \lambda_1)$ and $\bar{u}(p', \lambda_3)$ in the center of mass frame ³, where λ_i ($i = 1, 2, 3$) stand for helicity quantum numbers of initial nucleon, photon and final nucleon, in order. For each set of helicity quantum numbers, denoted by $H_s \equiv \{\lambda_1 \lambda_2 \lambda_3\}$, there is a helicity amplitude $\mathcal{M}_{H_s}^I$, which can be expanded as ⁴

$$\mathcal{M}_{H_s}^I(s, t) = 16\pi \sum_{J=M}^{\infty} (2J+1) \mathcal{M}_{H_s}^{IJ}(s) d_{\lambda\lambda'}^J(\theta), \quad (28)$$

where $M = \lambda$, $\lambda \equiv \lambda_1 - \lambda_2$ and $\lambda' \equiv \lambda_3$. $d^J(\theta)$ is the standard Wigner d -function. By imposing the orthonormal properties of the d^J functions, the partial wave helicity amplitudes $\mathcal{M}_{H_s}^{IJ}(s)$ in the above equation may be projected, i.e.

$$\mathcal{M}_{H_s}^{IJ}(s) = \frac{1}{32\pi} \int_{-1}^1 d \cos \theta \mathcal{M}_{H_s}^I(s, t) d_{\lambda\lambda'}^J(\theta). \quad (29)$$

The partial wave amplitude with $I = \frac{1}{2}$, $J = \frac{1}{2}$ and $L = 0$ (denoted by S_{11} in L_{2I2J} convention) is obtained via

$$\mathcal{M}(S_{11}) = \left(\mathcal{M}_{+++}^{I=\frac{1}{2}J=\frac{1}{2}} + \mathcal{M}_{++-}^{I=\frac{1}{2}J=\frac{1}{2}} \right), \quad (30)$$

which carry certain parity ⁵ and the helicity indices $\lambda_i = \pm \frac{1}{2}$ or ± 1 are abbreviated by \pm .

3.4 Singularities of partial wave amplitudes

3.4.1 The analytic structure of partial wave amplitudes

To illustrate the analytic structure of the partial wave amplitudes, we rewrite the partial wave projection formula in Eq. (29) in the following form

$$\mathcal{M}_{H_s}^{IJ}(s) = \frac{1}{32\pi} \int_{t_{\min}}^{t_{\max}} \sum_{i=1}^4 [(\mathcal{G}_{H_s}^J)_i \mathcal{A}_i^I(s, t)] dt, \quad (31)$$

where the invariant amplitude $\mathcal{M}_{H_s}^I$ has replaced by its Lorentz-decomposed expression given in Eq. (16) and t_{\min} , t_{\max} correspond to $\cos \theta = \pm 1$ through Eq. 33. Furthermore, the scalar functions $(\mathcal{G}_{H_s}^J)_i$ ($i = 1, \dots, 4$) are defined by

$$(\mathcal{G}_{H_s}^J)_i \equiv \bar{u} L_\mu^i u \epsilon^\mu \frac{d_{\lambda_1 \lambda'}^J(s, t)}{s \rho_{\pi N} \rho_{\gamma N}}, \quad (32)$$

³The spinor satisfies $\vec{\Sigma} \cdot \frac{\vec{p}}{|\vec{p}|} u_\pm(p) = \pm u_\pm(p)$, and polarization vector satisfies $\epsilon_\pm(q) = \frac{1}{\sqrt{2}} (\epsilon_1(q) \pm i\epsilon_2(q))$.

⁴It is worth stressing that there are in total 8 helicity amplitudes, nevertheless, only 4 of them are independent thanks to symmetries under parity and time reversion transformation.

⁵The positive direction particle is the direction of nucleon and the negative direction state is defined through $|-p_z, \lambda\rangle = e^{-i\pi J_z} e^{-i\pi J_y} |p_z, \lambda\rangle$, which differs in a phase with the case in Ref. [44].

where L_μ^i can be found in Eq. (17). In what follows, we proceed to discuss the analytic structure with the help of Eq. (31). Note here that the Mandelstam variable t is related to the cosine of the scattering angle θ via

$$t = 2m_N^2 - \frac{(s + m_N^2)(s + m_N^2 - m_\pi^2)}{2s} + s\rho_{\pi N}\rho_{\gamma N} \frac{\cos\theta}{2}. \quad (33)$$

On the one hand, It should be emphasized that the functions $(\mathcal{G}_{H_s}^J)_{i=\dots ts,4}$ rely merely on the kinematical structures of the scattering amplitudes, regardless of the dynamics of the system under consideration. Therefore, they are model-independent and can be calculated straightforwardly for any partial wave quantum numbers of J . In Appendix A, for $J = 1/2$ and $H_s = \{+-, +++, \dots\}$, all the explicit expressions of $(\mathcal{G}_{H_s}^J)_i$ are listed for the sake of easy reference. It can be observed that $(\mathcal{G}_{H_s}^{J=\frac{1}{2}})_i$ in S_{11} channel are just polynomials of t .

On the other hand, information on the dynamics are completely encoded in the scalar amplitudes $\mathcal{A}_i^J(s, t)$. In our tree-level ChPT calculation, they are represented by the results shown in Subsection 3.2, which are composed of contact terms, t -channel pion-pole, s - and u -channel nucleon-exchange contributions. The contact term and s -channel nucleon exchange term are polynomials of t , while t - and u -channel pole terms⁶ can be unified to a single type, $1/(t - c)$, with c a function of s .

Restricted to our tree-level calculation and with the above discussions, one can conclude there exist only one master integral:

$$\int_{t_{\min}}^{t_{\max}} \frac{t}{t - c} dt = t_{\max} - t_{\min} + c [\ln(t_{\max} - c) - \ln(t_{\min} - c)]. \quad (34)$$

All other integrals are either trivial in the sense that they are integrations over polynomials of t , being able to be reduced to the above integral by making use of the identity $\frac{t^n}{t-c} = t^{n-1} + \frac{ct^{n-1}}{t-c}$ with n a positive integer. In our current case, the constant c has three options, i.e., $c \in \{m_\pi^2, s - m_N^2 - m_\pi^2, 2s - 2m_N^2 - m_\pi^2\}$, which result in three typical logarithms $\mathcal{D}_i(s)$ after applying Eq. (34). We refer the readers to Appendix A for their explicit expressions. For the $\mathcal{D}_i(s)$ except $\mathcal{D}_3(s)$, which comes from kinematical decomposition, it should be mentioned that those logarithms are stemmed from the dynamics term $1/(t - c)$, while their composite arguments could be square root functions originated from the kinematical limits of the integrations. The logarithms and square root functions give rise to the partial-wave singularities to be discussed in the following subsections.

3.4.2 Dynamical singularities

The generic dynamical singularities of the partial-wave photoproduction amplitude have been discussed in detail in Ref. [37]. All possible singularities are displayed in Fig. 3 and are briefly illustrated in the following.

⁶ $\frac{1}{P \cdot q}$ due to kinematical decomposition can be transformed into this kind of form.

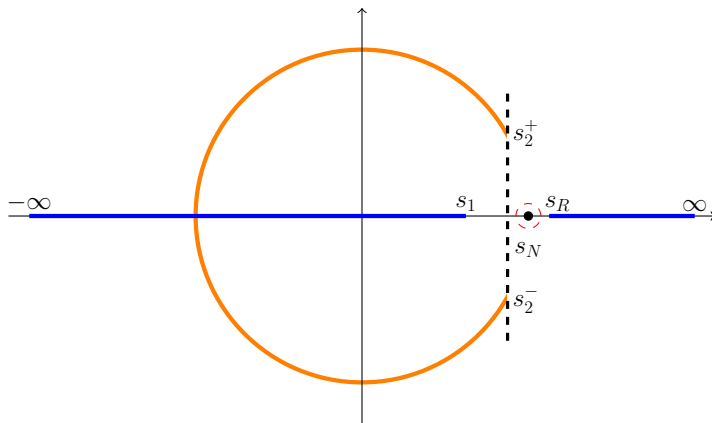


Figure 3: Dynamical Singularities. $s_N = m_N^2$, $s_1 = \frac{m_N}{m_\pi + m_N} (m_N^2 - m_N m_\pi - m_\pi^2)$.

- unitarity cut: $s \in [s_R, \infty)$ on account of the s -channel continuous spectrum.
- u -channel crossed cut: $s \in (-\infty, s_1]$ with $s_1 = \frac{m_N}{m_\pi + m_N} (m_N^2 - m_N m_\pi - m_\pi^2)$ due to the u -channel continuous spectrum for $u \geq (m_N + m_\pi)^2$.
- t -channel crossed cut: I. The arc, with branch points located at $s_2^\pm = m_N^2 - \frac{3}{2}m_\pi^2 \pm \frac{i}{2}m_\pi \sqrt{\frac{44}{5}m_N^2 - 9m_\pi^2}$, stems from t -channel continuous spectrum for $4m_\pi^2 \leq t \leq 4m_N^2$; ⁷ II. The t -channel continuous spectrum above $4m_N^2$ yields the cut $s \in (-\infty, 0]$.
- Trivial cut: $s \in (-\infty, 0]$ generated by the logarithms.
- Discrete term: located at $s = m_N^2 \equiv s_N$ and induced by the t -channel single pion exchange as well as the u -channel single nucleon exchange. ⁸.

Let us come back to our special case under consideration. Since the continuous spectrums are absent for a tree-level calculation, we meet only with the dynamical singularities of the trivial cut and the discrete term.

3.4.3 Kinematical singularities

Aside from the above-mentioned dynamical singularities, there exist additional kinematical singularities for an inelastic scattering process with spinors. The kinematical singularities are caused by the square-root and/or logarithmic functions appearing in the partial wave amplitudes. Kinematical cuts are introduced when the arguments of those two kinds of functions are negative. All the involved arguments together with their corresponding negative domains are listed in Table 1.

⁷This arc is not a circle arc. See Ref. [37] for detailed discussion.

⁸Actually, this isolated branch point singularity disappears after appropriately arranging the logarithms in the partial wave amplitudes. However, a singularity at m_N^2 will still be there due to kinematical properties, which will be discussed in the next subsection.

Table 1: Arguments causing singularities

Arguments	Negative Domain
$s - s_R$	$(-\infty, s_R)$
$s - s_L$	$(-\infty, s_L)$
s	$(-\infty, 0)$
$s + m_N^2 - m_\pi^2 - \sqrt{s - s_R}\sqrt{s - s_L}$	-
$s + m_N^2 - m_\pi^2 + \sqrt{s - s_R}\sqrt{s - s_L}$	$(-\infty, 0)$
$3s + m_N^2 - m_\pi^2 - \sqrt{s - s_R}\sqrt{s - s_L}$	$(-\infty, \frac{1}{2}(m_\pi^2 - 2m_N^2))$
$3s + m_N^2 - m_\pi^2 + \sqrt{s - s_R}\sqrt{s - s_L}$	$(-\infty, 0)$
$s - m_N^2 + m_\pi^2 - \sqrt{s - s_R}\sqrt{s - s_L}$	$(0, s_L)$
$s - m_N^2 + m_\pi^2 + \sqrt{s - s_R}\sqrt{s - s_L}$	$(-\infty, s_L)$

It should be pointed out that how these functions are organized in the way that does not affect the value in the physical region but may affect the values in complex plane. Here we give an example to illustrate it:

$\sqrt{(s - s_R)(s - s_L)}$ **Case:** There are two cuts. One goes from s_L to s_R and the other is an infinitely-long line, which is perpendicular to the real axis and passes the midpoint of s_L and s_R .

$\sqrt{s - s_R}\sqrt{s - s_L}$ **Case:** There is just one cut stretching from s_L to s_R with the cuts below s_L cancelling each other.

Meanwhile the values in the physical region in the above two cases are the same. In practice, we choose to expand the root functions in terms of power series and then continue them to the full complex plane. In this way, all the kinematical singularities represent themselves as cuts lying on real axis. And the logarithm functions in the form of $\ln \frac{a}{b}$, whose arguments contain root functions, are recast to $\ln a - \ln b$ in order to avoid the circular cut in the complex plane.

For the S_{11} channel, the cut between s_L and s_R disappears since $\mathcal{M}_{+++}^{I=\frac{1}{2}J=\frac{1}{2}}$ and $\mathcal{M}_{++-}^{I=\frac{1}{2}J=\frac{1}{2}}$ are conjugated with each other in this interval and this is not hard to be understood in observation of the explicit form of $(\mathcal{G}_{H_s}^J)_i$ in Appendix A. In addition, there is a pole-like singularity at m_N^2 coming from the fact that $\lim_{s \rightarrow m_N^2} \frac{\mathcal{D}_i}{\rho_{\gamma-N}}$, where the source of $\frac{1}{\rho}$ can be seen in Eq. (31), diverge, meanwhile the limit of $\lim_{s \rightarrow s_R} \frac{\mathcal{D}_i}{\rho_{\gamma-N}}$ is finite. But this pole-like singularity appearing in the amplitude can be viewed as the branch point of the left hand cut starting from m_N^2 in \mathcal{S} matrix since $S_{\gamma\pi} = \sqrt{\rho_{\gamma N} \rho_{\pi N} T}$, where $S_{\gamma\pi}$ is pion photoproduction \mathcal{S} matrix, or the branch point of electromagnetic unitarity cut of amplitudes. The results of additional singularity in S_{11} channel are displayed in Figure 4.

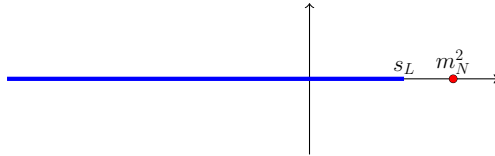


Figure 4: Kinematical Singularities

As the result of kinematical singularities, we should include s -channel and contact diagrams besides t - and u -channel resonance exchanges in the estimation of \mathcal{M}_L at tree level.

4 Numerical results and discussions

We are now in the position to compare the dispersive representation of photoproduction amplitude given in Eq. (8) with experimental multipole amplitude data from Ref. [38] in S_{11} channel. Based on our fitting results, the couplings of $N^*(890)$ to γN and πN can be extracted.

4.1 The fitting procedure

In our fitting procedure, there are three different kinds of parameters in Eq. (8): the LECs involved in determination of $\mathcal{M}_L(s)$, the subtraction constants in the auxiliary function $\mathcal{D}(s)$ and the ones in the overall subtraction polynomial $\mathcal{P}(s)$. Firstly, the parameters in the Lagrangian appearing in $\mathcal{M}_L(s)$ are chosen to be $m_N = 0.9383$ MeV, $m_\pi = 0.1396$ MeV, $e = 0.303$, $g_A = 1.267$, $F_\pi = 92.4$ MeV, $c_6 = 3.706/(4m_N)$ and $c_7 = -0.12/(2m_N)$ ⁹. Secondly, we set $\tilde{\mathcal{P}}(s) = 1$ and compute $\mathcal{D}(s)$ by using the S_{11} -wave phase shift extracted from the πN S matrix given in Ref. [19]. Two solutions of the πN S matrix are adopted: one corresponding to $s_c = -1$ GeV² and the other to $s_c = -9$ GeV² with s_c being a cut off parameter therein. Note that it should be a good approximation for a single-channel case that the integrations in Eqs. (10) and (8) are performed up to 2.095GeV² rather than to infinity. Lastly, the constants in the \mathcal{P} are left as fitting parameters.¹⁰ Here we only consider two fit cases: Fit I with $\mathcal{P}(s) = a$ and Fit II $\mathcal{P}(s) = a + b s$ while the subtraction points are set to be zero.

We perform a fit to the data points on the multipole amplitudes¹¹, which are traditionally denoted by S_{11} with suffixes of target type (n or p) and electromagnetic transition (E :electric, M :magnetic), from πN threshold to 1.440 GeV² just below the peak of $\Delta(1232)$. The fit results for both proton (p) and neutron (n) targets are displayed in Figures 5 and 6, respectively. For comparison, in Fig. 5 and Fig. 6, we also show the $\mathcal{O}(q^2)$ chiral results of the real parts of multipole amplitudes. As expected, the chiral results only describe the data very well at low energies close to threshold. The values of the fit parameters are collected in Table 2.

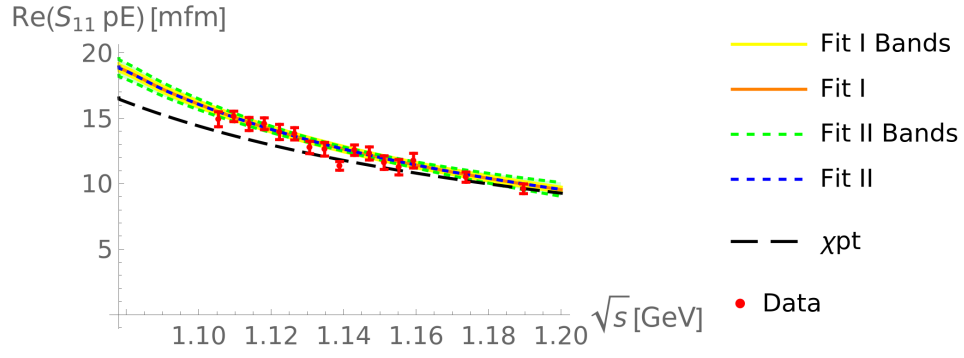
⁹Neglecting ChPT correction beyond tree level, the two LECs c_6 and c_7 can be related to the anomalous magnetic moments of the nucleon via

$$c_6 = \frac{k_p + k_n}{2m_N}, c_7 = \frac{k_p - k_n}{4m_N}, \quad (35)$$

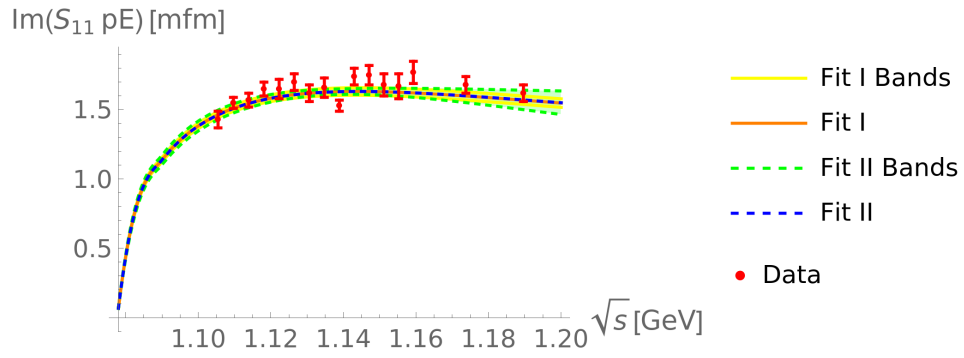
with k_p and k_n being anomalous magnetic moments of proton and neutron, respectively. Since k_p and k_n are precisely determined by experiments [42], one can infer the uncertainties of c_6 and c_7 must be negligible and shall hardly change our results.

¹⁰ $\tilde{\mathcal{P}}$ can always be chosen to be 1 in Eq. (6).

¹¹The relation between multipole amplitudes and our amplitudes can be established through traditional CGLN convention, which can be found in Appendix B.



(a) Real Part



(b) Imaginary Part

Figure 5: p Target. Upper panel: real part of the S_{11} electric multipole; Lower panel: imaginary part of the S_{11} electric multipole. The solid orange and dashed blue lines represent our dispersive descriptions based on Fit I and Fit II, respectively. Yellow solid line and green dashed line represent the error bands of Fit I and Fit II. For comparison, the chiral result of the real part of the multipole is also shown, corresponding to the black long dashed line.

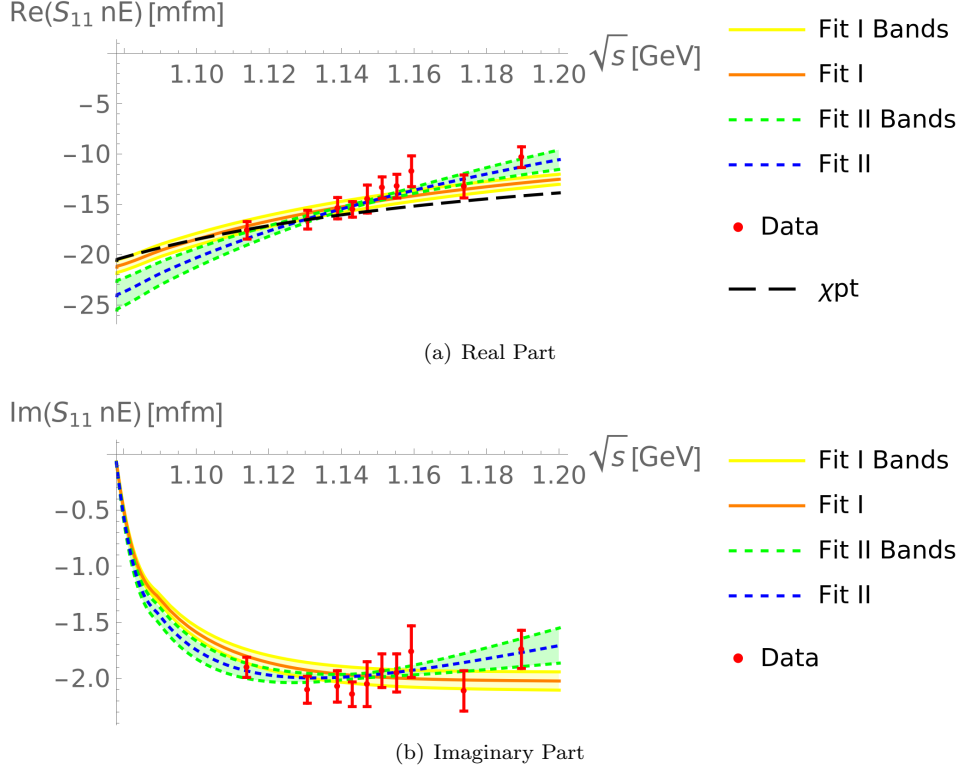


Figure 6: n Target. Same definitions as in Fig. 5

Table 2: Results of the fit parameters. a is dimensionless and the unit of b is GeV^{-1} .

Target	Case	Parameter	Value	$\chi^2/d.o.f$
p	Fit I	$10^2 \times a$	-0.0712 ± 0.1334	1.58
	Fit II	$10^2 \times a$	0.0287 ± 3.2525	1.63
		$10^2 \times b$	-0.210 ± 2.504	
n	Fit I	$10^2 \times a$	-1.43 ± 0.35	1.22
	Fit II	$10^2 \times a$	12.50 ± 6.90	0.643
		$10^2 \times b$	-10.4 ± 5.2	

For Fit I, our results are in good agreement with the experimental data in the sense that the averaged χ^2 are close to one, $\chi^2/d.o.f = 1.58$ for the p target and $\chi^2/d.o.f = 1.22$ for the n target. As can be seen from Table 2, the modulus of the central value of a is close to zero in the proton target case, while it is 1.43 in the neutron target case. That is due to the fact that the electric multipoles calculated from BChPT in the proton case can already well describe the experimental data, enforcing a nearly-zero contribution from the subtraction polynomial in the fitting procedure and further resulting a nearly-zero value of a . However, in the neutron case the discrepancy between BChPT results and experimental data are larger compared to the proton case, which leads to a larger central value (modulus) of a subsequently.

Fit II is performed by using a rank-2 subtraction polynomial with two parameters a and b . Compared to Fit I, the qualities of Fit II are improved, which is under our expectation since one

more free parameter is involved in the fit procedure. However, the fitting parameters a and b of Fit II are highly correlated with a correlation coefficient which is nearly -1 . Thus, Fit I is more advisable.

4.2 Analytic continuation and extraction of the $N^*(890)$ couplings

In the above subsection, all the involved parameters in the dispersive S -wave photoproduction amplitude $\mathcal{M}(s)$ have been determined. Since $N^*(890)$, as a subthreshold resonance, is located on the second Riemann sheet (RS), one needs to perform analytic continuation in order to extract its couplings to the γN and πN systems.

The amplitude on the second RS can be deduced via

$$\mathcal{M}^{\text{II}}(s) = \frac{\mathcal{M}(s)}{\mathcal{S}(s)}, \quad (36)$$

where $\mathcal{M}(s)$ is the partial-wave photoproduction amplitude given in Eq. (8) and $\mathcal{S}(s)$ corresponds to the S matrix of πN scattering with same quantum numbers as $\mathcal{M}(s)$. If there exists a second RS pole located at z_R , the S matrix can be approximated by

$$\mathcal{S}(s) \approx \mathcal{S}'(z_R)(s - z_R) \quad (37)$$

in the vicinity of z_{II} . Thus,

$$\mathcal{M}^{\text{II}}(s) = \frac{\mathcal{M}(s)}{\mathcal{S}'(z_R)(s - z_R)}. \quad (38)$$

On the other hand, the couplings of this second RS pole to the γN and πN systems are defined as the residue via

$$\mathcal{M}^{\text{II}}(s \rightarrow z_R) = \frac{g_\gamma g_\pi}{s - z_R}, \quad (39)$$

with g_γ and g_π denoting the γN and πN couplings, respectively. Compared to Eq. (38), one obtains

$$g_\gamma g_\pi = \frac{\mathcal{M}(z_R)}{\mathcal{S}'(z_R)}. \quad (40)$$

The πN coupling can also be extracted from elastic πN scattering, i.e.,

$$g_\pi^2 = \frac{\mathcal{T}(z_R)}{\mathcal{S}'(z_R)}, \quad (41)$$

where \mathcal{T} is the corresponding partial-wave πN scattering amplitude.

Now we proceed with the numerical calculation of the couplings of $N^*(890)$. According to Eqs. (40) and (68), the pion photoproduction $N^*(890)$ residue couplings, i.e. $g_\gamma g_\pi$, can be extracted from multipole amplitudes. In the meantime, g_π^2 can be computed by using Eq. (41), which was already done in Ref. [19]. Results of the couplings are listed in Table 3. The results based on Fit II are also shown to check the stability of the obtained values. We employed two solutions of the pole position of the $N^*(890)$, $\sqrt{s} = 0.882 - 0.190i$ corresponding to the cutoff $s_c = -1$ GeV and $\sqrt{s} = 0.960 - 0.192i$ to $s_c = -9$ GeV; See Ref. [19] for detailed explanation.

Table 3: Results of $g_\gamma g_\pi$ and g_π^2 . Pole position, moduli and phase are in GeV, $10^{-2} \times \text{GeV}^2$ and degrees, in order. g_π^2 are the same for p target and n target due to the isospin symmetry.

Target	$g_\gamma g_\pi$						g_π^2	
	Fit I			Fit II			Moduli	Phase
	Pole Position	Moduli	Phase	Moduli	Phase	Moduli	Phase	
p	$0.882 - 0.190i$	(1.212 ± 0.014)	-79.2 ± 1.3	1.203 ± 0.302	-78.9 ± 11.4	19.7 ± 0.3	32.6 ± 1.0	
	$0.960 - 0.192i$	(1.467 ± 0.016)	-71.3 ± 0.9	1.459 ± 0.279	-71.2 ± 3.5	21.4 ± 0.2	33.6 ± 0.8	
n	$0.882 - 0.190i$	(0.6416 ± 0.0265)	111 ± 7	2.025 ± 0.731	81.4 ± 6.9			
	$0.960 - 0.192i$	(1.111 ± 0.050)	103 ± 3	2.342 ± 0.605	98.0 ± 1.5			

In the extraction of $g_\gamma g_\pi$ and g_π^2 of $N^*(890)$, z_R is treated as the $N^*(890)$ pole position in the s plane, $\mathcal{M}(z_R)$ can be obtained from the dispersion relation in Eq. (8) once \mathcal{P} is determined, $\mathcal{T}(z_R)$ can be obtained through $\mathcal{S}(z_R) = 1 + 2i\rho_{\pi N}\mathcal{T} = 0$ and $\frac{1}{S'(z_R)}$ is just the residue of S^{II} from Ref. [19]. But in order to compare the results of $N^*(1535)$, which are extracted directly from multipole amplitudes parameterized in \sqrt{s} plane in Ref. [39], the conventions should be consistent. In S_{11} channel the following equation can be used to translate these residues from different conventions into residues directly extracted from multipole amplitudes in s plane.

$$E_{0+}^{I=\frac{1}{2}} \Pi(s \rightarrow z_R) = -\sqrt{\frac{2}{3s}} \frac{g_\gamma g_\pi}{s - z_R} = -\sqrt{\frac{2}{3s}} \frac{g_\gamma g_\pi}{2\sqrt{z_R}(\sqrt{s} - \sqrt{z_R})}, \quad (42)$$

where R stands for $N^*(890)$ or $N^*(1535)$. In S_{11} pE the moduli of residue is $2.41\text{mfm} \cdot \text{GeV}^2$ with phase 120° , meanwhile the magnitude of $N^*(1535)$ residue coupling from Ref. [39] is about $0.736\text{mfm} \cdot \text{GeV}^2$ and phase is -27° . One can see the magnitude of the $N^*(890)$ residue is larger than that of the $N^*(1535)$ residue. The $|g_\pi^2|$ of $N^*(890)$ is 0.2GeV^2 , and the one of $N^*(1535)$, which is obtained by the value in Ref. [45], is 0.08GeV^2 . The g_π^2 of these two resonances may account for part of the reason why $N^*(890)$ photoproduction residue is large, and using above results g_γ of these two resonances can be obtained. The $|g_\gamma|$ of $N^*(890)$ is 0.032GeV meanwhile the one of $N^*(1535)$ is 0.024GeV and one can see the magnitudes are almost the same. One should notice that the results of n target are quiet unstable. The fact that data points are few and they have large error bars may account for the main reason.

We can also calculate the decay amplitudes $\mathcal{A}^{\frac{1}{2}}$ at the $N^*(890)$ pole position, which is related to the coupling g_γ , using the formula given in Ref. [39]:

$$\mathcal{A}^{\frac{1}{2}} = g_\gamma \sqrt{\frac{\pi}{q_r^2 m_N}} \rho_{\gamma N}, \quad (43)$$

where q_r is modulus of the photon momentum calculated at the resonance pole position.

Furthermore, we can obtain the partial widths of the $N^*(890) \rightarrow \gamma N$ channel at the pole by following the next formula, which is from Ref. [46] and converted to our convention.

$$\Gamma_{\gamma N} = \left| \rho_{\gamma N} \frac{g_\gamma^2}{\sqrt{z_R}} \right|, \quad (44)$$

where z_R is treated as $N^*(890)$ pole position. The values of the decay amplitudes $\mathcal{A}^{\frac{1}{2}}$ and the partial decay width at the pole $\Gamma_{\gamma N}$ are collected in Table 4.

Table 4: Values of the decay amplitude ($\mathcal{A}^{\frac{1}{2}}$) and decay width ($\Gamma_{\gamma N}$) calculated at the $N^*(890)$ pole position. Phase, $\mathcal{A}^{\frac{1}{2}}$ and $\Gamma_{\gamma N}$ are in degrees, $\text{GeV}^{-\frac{1}{2}}$ and MeV, respectively.

Target	Pole Position	$\mathcal{A}^{\frac{1}{2}}$				$\Gamma_{\gamma N}$	
		Fit I		Fit II		Fit I	Fit II
		Moduli	Phase	Moduli	Phase		
p	$0.882 - 0.190i$	0.165 ± 0.004	-129 ± 2	0.165 ± 0.043	-129 ± 12	0.369 ± 0.014	0.363 ± 0.210
	$0.960 - 0.192i$	0.191 ± 0.004	-43.4 ± 1.4	0.191 ± 0.038	-43.3 ± 3.9	0.396 ± 0.013	0.391 ± 0.168
n	$0.882 - 0.190i$	0.0879 ± 0.0043	61.7 ± 8.2	0.277 ± 0.102	31.4 ± 7.4	0.103 ± 0.011	1.03 ± 0.89
	$0.960 - 0.192i$	0.145 ± 0.008	130 ± 4	0.305 ± 0.096	125 ± 3	0.227 ± 0.023	1.01 ± 0.73

The $|\mathcal{A}^{\frac{1}{2}}|$ of $N^*(890)$ is larger than the one of $N^*(1535)$, which is $0.074\text{GeV}^{-\frac{1}{2}}$ with the phase being -17° in $S_{11}\text{pE}$ from Ref. [39] but the decay widths at the pole are almost the same regardless of the instability of n target results.

5 Summary

In this paper, we have performed a careful dispersive analysis of the process of single pion photon production off the nucleon, in the S_{11} wave of the final pion-nucleon system. In such a dispersive representation, the right-hand cut contribution can be related to an Omnés solution, which takes the elastic πN phase shifts as inputs, and hence is known up to a polynomial. On the other hand, we estimate the left-hand cut contribution by making use of the $\mathcal{O}(q^2)$ tree amplitudes taken from chiral perturbation theory. A detailed discussion on how to establish a proper analytic structure of the partial-wave pion photon production amplitude is also presented for easy reference in future. To pin down the free parameters in the dispersive amplitude, we perform fits to experimental data of multipole amplitudes in the channels indicated by $S_{11}\text{pE}$ and $S_{11}\text{nE}$ for the energies ranging from πN threshold to 1.440 GeV^2 .

It is found that the experimental data can be well described by the dispersive amplitude with only one free subtraction parameter. We then continue the dispersive amplitude to the second Riemann sheet for the purpose of being able to extract the couplings of N^* to the γN and πN systems, which are denoted by g_γ and g_π , respectively. Based on the obtained value of $g_\gamma g_\pi$, the modulus of the corresponding residue of the multipole amplitude ($S_{11}\text{pE}$) at the $N^*(890)$ pole position turns out to be $2.41\text{mfm} \cdot \text{GeV}^2$, which is much larger than the modulus of the residue of $N^*(1535)$, i.e. $0.736\text{mfm} \cdot \text{GeV}^2$ [39]. That means the strength of the interaction of $N^*(890)$ with πN system is stronger, compared to the one regarding $N^*(1535)$. Its physically reasonable and within expectation since $N^*(890)$ is supposed to be composed of πN system and $N^*(1535)$ has tiny coupling with πN as we all know. The results provides further evidence of existence of $N^*(890)$. As byproducts, the decay amplitude and the decay width at the $N^*(890)$ pole position \mathcal{A}_h and the $\Gamma_{\gamma N}$ are obtained for future reference.

Acknowledgments

This work is supported by National Nature Science Foundations of China (NSFC) under Contract number 11905258, 11975028 and 10925522, and by the Fundamental Research Funds for the Central Universities under No. 531118010379. The authors are grateful to Y. F. Wang for valuable advises.

Appendices

A Partial wave amplitude

The functions $(\mathcal{G}_{H_s}^J)_i$ defined in Eq. (32) are shown for S_{11} wave in the following:

$$(\mathcal{G}_{+++}^{J=\frac{1}{2}})_1 = ik_1 \sqrt{s} (k_l k_r (m_N^2 - s) - m_N^2 (m_\pi^2 + 2s) + m_N^4 + s (-m_\pi^2 + s + 2t)) \times ((m_N^2 - s) ((m_N - m_\pi)^2 - s) ((m_N + m_\pi)^2 - s))^{-1}, \quad (45)$$

$$(\mathcal{G}_{++-}^{J=\frac{1}{2}})_1 = -ik_2 \sqrt{s} (k_l k_r (s - m_N^2) - m_N^2 (m_\pi^2 + 2s) + m_N^4 + s (-m_\pi^2 + s + 2t)) \times ((m_N^2 - s) ((m_N - m_\pi)^2 - s) ((m_N + m_\pi)^2 - s))^{-1}, \quad (46)$$

$$(\mathcal{G}_{+++}^{J=\frac{1}{2}})_2 = is (k_1 \sqrt{s} - k_2 m_N) (m_N^2 (m_\pi^4 - t (m_\pi^2 + 2s)) + t m_N^4 + s (-m_\pi^2 + s + t)) \times ((m_N^2 - s)^2 ((m_N - m_\pi)^2 - s) ((m_N + m_\pi)^2 - s))^{-1}, \quad (47)$$

$$(\mathcal{G}_{++-}^{J=\frac{1}{2}})_2 = is (k_1 m_N - k_2 \sqrt{s}) (m_N^2 (m_\pi^4 - t (m_\pi^2 + 2s)) + t m_N^4 + s (-m_\pi^2 + s + t)) \times ((m_N^2 - s)^2 ((m_N - m_\pi)^2 - s) ((m_N + m_\pi)^2 - s))^{-1}, \quad (48)$$

$$(\mathcal{G}_{+++}^{J=\frac{1}{2}})_3 = -k_2 (m_N^2 (k_l k_r - m_\pi^2 - 2s) + s (-k_l k_r - m_\pi^2 + s + 2t) + m_N^4) \times \left[k_l k_r \left(\frac{2k_1 \sqrt{s} m_N (m_\pi^2 - t)}{k_2} - m_N^2 (m_\pi^2 + 2s) + m_N^4 + s (m_\pi^2 + s) \right) - (m_N^2 - s) ((m_N - m_\pi)^2 - s) ((m_N + m_\pi)^2 - s) \right] \times (4 (m_N^2 - s)^2 (s - (m_N - m_\pi)^2)^{3/2} (s - (m_N + m_\pi)^2)^{3/2})^{-1}, \quad (49)$$

$$(\mathcal{G}_{++-}^{J=\frac{1}{2}})_3 = k_1 (-m_N^2 (k_l k_r + m_\pi^2 + 2s) + s (k_l k_r - m_\pi^2 + s + 2t) + m_N^4) \times \left[k_l k_r \left(\frac{2\sqrt{s} m_N (m_\pi^2 - t) k_2}{k_1} - m_N^2 (m_\pi^2 + 2s) + m_N^4 + s (m_\pi^2 + s) \right) + (m_N^2 - s) ((m_N - m_\pi)^2 - s) ((m_N + m_\pi)^2 - s) \right] \times (4 (m_N^2 - s)^2 (s - (m_N - m_\pi)^2)^{3/2} (s - (m_N + m_\pi)^2)^{3/2})^{-1}, \quad (50)$$

$$(\mathcal{G}_{+++}^{J=\frac{1}{2}})_4 = (k_l k_r (m_N^2 - s) - m_N^2 (m_\pi^2 + 2s) + m_N^4 + s (-m_\pi^2 + s + 2t)) \times \left[k_2 k_l k_r (-2\sqrt{s} m_N (-m_\pi^2 + 2s + t) - m_N^2 (m_\pi^2 - 2s) + m_N^4 + s (m_\pi^2 - 3s)) + 4k_1 \sqrt{s} k_l k_r m_N^3 - k_2 (m_N^2 - s) ((m_N - m_\pi)^2 - s) ((m_N + m_\pi)^2 - s) \right] \times (4 (m_N^2 - s)^2 (s - (m_N - m_\pi)^2)^{3/2} (s - (m_N + m_\pi)^2)^{3/2})^{-1}, \quad (51)$$

$$(\mathcal{G}_{++-}^{J=\frac{1}{2}})_4 = (k_l k_r (m_N^2 - s) + m_N^2 (m_\pi^2 + 2s) - m_N^4 + s (m_\pi^2 - s - 2t)) \times$$

$$\begin{aligned}
& \left[2k_2 \sqrt{s} k_l k_r m_N (2m_N^2 + m_\pi^2 - 2s - t) + k_1 (m_N^2 - s) \times \right. \\
& \left. (k_l k_r (m_N^2 - m_\pi^2 + 3s) - 2m_N^2 (m_\pi^2 + s) + m_N^4 + (m_\pi^2 - s)^2) \right] \times \\
& \left(4 (m_N^2 - s)^2 (s - (m_N - m_\pi)^2)^{3/2} (s - (m_N + m_\pi)^2)^{3/2} \right)^{-1} \quad (52)
\end{aligned}$$

with

$$\begin{aligned}
k_l &= \sqrt{s - s_L} \ , \\
k_r &= \sqrt{s - s_R} \ , \\
k_1 &= \sqrt{s + m_N^2 - m_\pi^2 - \sqrt{s - s_R} \sqrt{s - s_L}} \ , \\
k_2 &= \sqrt{s + m_N^2 - m_\pi^2 + \sqrt{s - s_R} \sqrt{s - s_L}} \ .
\end{aligned} \quad (53)$$

The amplitudes $A_i(s, t)$ up to $\mathcal{O}(q^2)$ contain following terms:

- t channel pion exchange: $\frac{1}{t - m_\pi^2}$;
- u channel nucleon exchange: $\frac{1}{u - m_N^2} = \frac{1}{m_N^2 + m_\pi^2 - s - t}$;
- Kinematical decomposition: $\frac{1}{P \cdot q} = \frac{4}{t - 2m_N^2 - m_\pi^2 + 2s}$.

They lead to logarithm terms:

$$\begin{aligned}
\mathcal{D}_1 &= \ln \left(-\sqrt{s - s_L} \sqrt{s - s_R} + m_N^2 - m_\pi^2 + s \right) \\
&\quad - \ln \left(\sqrt{s - s_L} \sqrt{s - s_R} + m_N^2 - m_\pi^2 + s \right) \ , \quad (54)
\end{aligned}$$

$$\begin{aligned}
\mathcal{D}_2 &= \ln \left(-\sqrt{s - s_L} \sqrt{s - s_R} - m_N^2 + m_\pi^2 + s \right) \\
&\quad - \ln \left(\sqrt{s - s_L} \sqrt{s - s_R} - m_N^2 + m_\pi^2 + s \right) \ , \quad (55)
\end{aligned}$$

$$\begin{aligned}
\mathcal{D}_3 &= \ln \left(\sqrt{s - s_L} \sqrt{s - s_R} + m_N^2 - m_\pi^2 + 3s \right) \\
&\quad - \ln \left(-\sqrt{s - s_L} \sqrt{s - s_R} + m_N^2 - m_\pi^2 + 3s \right) \ . \quad (56)
\end{aligned}$$

B CGLN Amplitudes

Traditional pion photoproduction partial wave analysis is in CGLN amplitudes (\mathcal{F}) with

$$\frac{d\sigma}{d\Omega} = \frac{q'}{q} |\langle \chi_f | \mathcal{F} | \chi_i \rangle|^2 \ , \quad (57)$$

where $\chi_{i(f)}$ are Pauli spinor and

$$\mathcal{F} = i\vec{\sigma} \cdot \vec{\epsilon} \mathcal{F}_1 + \left(\vec{\sigma} \cdot \vec{q}' \right) \vec{\sigma} \cdot (\vec{q} \times \vec{\epsilon}) \mathcal{F}_2 + i(\vec{\sigma} \cdot q) \left(\vec{q}' \cdot \vec{\epsilon} \right) \mathcal{F}_3 + i \left(\vec{q}' \cdot \vec{\sigma} \right) \left(\vec{q}' \cdot \vec{\epsilon} \right) \mathcal{F}_4 \ , \quad (58)$$

where there are four independent amplitudes. The connection of our scattering amplitudes to \mathcal{F} can be obtained:

$$\mathcal{M}_{fi} = 8\pi \sqrt{s} \mathcal{F}_{fi} \ , \quad (59)$$

where the subscripts f , i mean initial and final states are substituted into Eq. 58 and we will omit it in the following discussion.

Furthermore, the partial wave amplitude \mathcal{F}^J is defined in Ref. [3]:

$$\mathcal{F}_{\pm;\lambda_r}^J = \frac{1}{4\pi} \int_{-1}^1 \int_0^{2\pi} F_{\pm;\lambda_r} D^J(\theta, \phi) d\Omega, \quad (60)$$

where \pm mean the final nucleon helicity and $\lambda_r = \frac{1}{2}$ or $\frac{3}{2}$, which is the moduli of initial helicity. Also, definite parity amplitudes can be obtained:

$$\begin{aligned} A_{n+} &= -\frac{1}{\sqrt{2}} \left(\mathcal{F}_{+,\frac{1}{2}}^J + \mathcal{F}_{-,\frac{1}{2}}^J \right), \\ A_{(n+1)-} &= \frac{1}{\sqrt{2}} \left(\mathcal{F}_{+,\frac{1}{2}}^J - \mathcal{F}_{-,\frac{1}{2}}^J \right), \\ B_{n+} &= \sqrt{\frac{2}{n(n+2)}} \left(\mathcal{F}_{+,\frac{3}{2}}^J - \mathcal{F}_{-,\frac{3}{2}}^J \right), \\ B_{(n+1)-} &= -\sqrt{\frac{2}{n(n+2)}} \left(\mathcal{F}_{+,\frac{3}{2}}^J - \mathcal{F}_{-,\frac{3}{2}}^J \right), \end{aligned} \quad (61)$$

where $A_{n\pm}, B_{n\pm}$ are amplitudes with $J = n \pm \frac{1}{2}$ and $P = -(-1)^n$.

According to Ref. [3], one can obtain the following relation between CGLN partial wave amplitudes ($A_{n\pm}$ and $B_{n\pm}$) and multipole amplitudes ($E_{n\pm}$ and $M_{n\pm}$):

$$E_{0+} = A_{0+}, \quad (62)$$

$$M_{1-} = A_{1-}. \quad (63)$$

and for $l \geq 1$

$$E_{l+} = (l+1)^{-1} \left(A_{l+} + \frac{1}{2} l B_{l+} \right), \quad (64)$$

$$M_{l+} = (l+1)^{-1} \left(A_{l+} - \frac{1}{2} (l+2) B_{l+} \right), \quad (65)$$

$$E_{(l+1)-} = - (l+1)^{-1} \left(A_{(l+1)-} - \frac{1}{2} (l+2) B_{(l+1)-} \right), \quad (66)$$

$$M_{(l+1)-} = (l+1)^{-1} \left(A_{(l+1)-} + \frac{1}{2} l B_{(l+1)-} \right). \quad (67)$$

Further, consider the fact that $E_{0+}^{I=\frac{1}{2}}$ isn't normalized in isospin space according to Refs. [47] and [48], so we have additional $\sqrt{3}$ in normalization factor, and the relation in S_{11} channel can be obtained:

$$E_{0+}^{I=\frac{1}{2}} = -\sqrt{\frac{2}{3s}} \mathcal{M}(S_{11}), \quad (68)$$

where $E_{0+}^{I=\frac{1}{2}}$ is conventional multipole amplitude with 0 and + refers to S wave and minus parity respectively.

References

- [1] G. F. Chew, M. L. Goldberger, F. E. Low, and Y. Nambu, Phys. Rev. **106**, 1345 (1957).
- [2] S. L. Adler, Annals Phys. **50**, 189 (1968), [,225(1968)].
- [3] R. L. Walker, Phys. Rev. **182**, 1729 (1969).
- [4] D. Drechsel, S. S. Kamalov, and L. Tiator, Eur. Phys. J. **A34**, 69 (2007).
- [5] P. Benz *et al.*, Aachen-Bonn-Hamburg-Heidelberg-Muenchen, Nucl. Phys. **B65**, 158 (1973).
- [6] M. Fuchs *et al.*, Phys. Lett. **B368**, 20 (1996).
- [7] G. Blanpied *et al.*, Phys. Rev. **C64**, 025203 (2001).
- [8] J. Ahrens *et al.*, GDH, A2, Eur. Phys. J. **A21**, 323 (2004).
- [9] INS Data Analysis Center, <http://gwdac.phys.gwu.edu/>.
- [10] V. Bernard, N. Kaiser, J. Gasser, and U. G. Meissner, Phys. Lett. **B268**, 291 (1991).
- [11] V. Bernard, N. Kaiser, and U. G. Meissner, Nucl. Phys. **B383**, 442 (1992).
- [12] V. Bernard, N. Kaiser, and U. G. Meissner, Eur. Phys. J. **A11**, 209 (2001).
- [13] M. Hilt, S. Scherer, and L. Tiator, Phys. Rev. **C87**, 045204 (2013).
- [14] M. Hilt, B. C. Lehnhart, S. Scherer, and L. Tiator, Phys. Rev. **C88**, 055207 (2013).
- [15] A. N. Hiller Blin, T. Ledwig, and M. J. Vicente Vacas, Phys. Lett. **B747**, 217 (2015).
- [16] A. N. Hiller Blin, T. Ledwig, and M. J. Vicente Vacas, Phys. Rev. **D93**, 094018 (2016).
- [17] G. H. Guerrero Navarro, M. J. Vicente Vacas, A. N. Hiller Blin, and D.-L. Yao, Phys. Rev. **D100**, 094021 (2019).
- [18] B. R. Martin, D. Morgan, G. L. Shaw, and G. Shaw, *Pion-pion Interactions in Particle Physics*, (Academic Press, London, 1976).
- [19] Y. F. Wang, D. L. Yao, and H. Q. Zheng, Chin. Phys. **C43**, 064110 (2019).
- [20] Y. F. Wang, D. L. Yao, and H. Q. Zheng, Front. Phys. **14**, 1 (2019).
- [21] Y. F. Wang, D. L. Yao, and H. Q. Zheng, Eur. Phys. J. **C78**, 543 (2018).
- [22] Y. H. Chen, D. L. Yao, and H. Q. Zheng, Phys. Rev. **D87**, 054019 (2013).
- [23] J. Alarcon, J. Martin Camalich, and J. Oller, Annals Phys. **336**, 413 (2013), 1210.4450.
- [24] D. L. Yao *et al.*, JHEP **05**, 038 (2016).
- [25] D. Siemens *et al.*, Phys. Rev. **C96**, 055205 (2017).
- [26] Z. G. Xiao and H. Q. Zheng, Nucl. Phys. **A695**, 273 (2001).
- [27] J. Y. He, Z. G. Xiao, and H. Q. Zheng, Phys. Lett. **B536**, 59 (2002), [Erratum: Phys. Lett. B549,362 (2002)].

- [28] H. Q. Zheng *et al.*, Nucl. Phys. **A733**, 235 (2004).
- [29] H. Q. Zheng, Z. Y. Zhou, G. Y. Qin, and Z. G. Xiao, AIP Conf. Proc. **717**, 322 (2004).
- [30] Z. Y. Zhou *et al.*, JHEP **02**, 043 (2005).
- [31] Z. Zhou and H. Zheng, Nucl. Phys. **A775**, 212 (2006).
- [32] Y. Ma, W. Q. Niu, Y. F. Wang, and H. Q. Zheng, (2020).
- [33] O. Babelon, J.-L. Basdevant, D. Caillerie, and G. Mennessier, Nucl. Phys. **B113**, 445 (1976).
- [34] O. Babelon, J.-L. Basdevant, D. Caillerie, M. Gourdin, and G. Mennessier, Nucl. Phys. **B114**, 252 (1976).
- [35] Y. Mao, X. G. Wang, O. Zhang, H. Q. Zheng, and Z. Y. Zhou, Phys. Rev. **D79**, 116008 (2009).
- [36] L. Y. Dai and M. R. Pennington, Phys. Rev. **D94**, 116021 (2016).
- [37] J. Kennedy and T. D. Spearman, Phys. Rev. **126**, 1596 (1962).
- [38] R. L. Workman, M. W. Paris, W. J. Briscoe, and I. I. Strakovsky, Phys. Rev. **C86**, 015202 (2012).
- [39] A. Švarc *et al.*, Phys. Rev. **C89**, 065208 (2014).
- [40] R. Omnès, Nuovo Cim. **8**, 316 (1958).
- [41] K. M. Watson, Phys. Rev. **95**, 228 (1954).
- [42] M. Tanabashi *et al.*, Particle Data Group, Phys. Rev. **D98**, 030001 (2018).
- [43] S. Scherer and M. R. Schindler, Lect. Notes Phys. **830**, 1 (2012).
- [44] M. Jacob and G. C. Wick, Annals Phys. **281**, 404 (2000).
- [45] R. A. Arndt, W. J. Briscoe, I. I. Strakovsky, and R. L. Workman, Phys. Rev. **C74**, 1 (2006).
- [46] R. L. Workman, L. Tiator, and A. Sarantsev, Phys. Rev. **C87**, 3 (2013).
- [47] R. A. Amdt, R. L. Workman, Z. Li, and L. D. Roper, Phys. Rev. **C42**, 1853 (1990).
- [48] A. Gasparyan and M. Lutz, Nucl. Phys. **A848**, 126 (2010).